Heliyon 10 (2024) e29955

Contents lists available at ScienceDirect

Heliyon

journal homepage: www.cell.com/heliyon

Research article

Correlation analysis between BRAF^{V600E} mutation and ultrasonic and clinical features of papillary thyroid cancer

Jiahao Wen [b,1], Haizhou Liu [a,c,1], Yanyan Lin [a,1], Zixuan Liang [b], Lili Wei [b], Qi Zeng [b], Shanshan Wei [d], Litu Zhang [a,c,**], Weiping Yang [b,*]

[a] Department of Research, Guangxi Medical University Cancer Hospital, Guangxi Medical University, Nanning, 530021, Guangxi Zhuang Autonomous Region, China
[b] Department of Ultrasound, Guangxi Medical University Cancer Hospital, Guangxi Medical University, Nanning, 530021, Guangxi Zhuang Autonomous Region, China
[c] Guangxi Cancer Molecular Medicine Engineering Research Center, Nanning, 530021, Guangxi Zhuang Autonomous Region, China
[d] Guangxi Medical University, Nanning, 530021, Guangxi Zhuang Autonomous Region, China

ARTICLE INFO

Keywords:
Papillary thyroid cancer
BRAF
Ultrasonic features
Nomogram

ABSTRACT

Purpose: The study investigates the value of the BRAF^{V600E} mutation in determining the aggressiveness of papillary thyroid cancer (PTC) and its correlation with ultrasound features.
Methods: The study selected 176 patients with BRAF^{V600E} mutation and 80 without the mutation who underwent surgery at Guangxi Medical University Cancer Hospital. Clinical and pathological data were collected, focusing on BRAF^{V600E} mutations and associated ultrasonic features. Correlation analysis, as well as univariate and multivariate logistic regression analysis, were conducted to identify independent risk factors for BRAF^{V600E} mutation. The results were verified using a nomogram model.
Results: The analysis results indicate that the BRAF^{V600E} mutation correlates with tumor size, nodule size, taller-than-wide shape, margin, and shape of papillary thyroid cancer. The receiver operating characteristic curve was used to analyze the diagnostic effect of these features on BRAF^{V600E} mutation. The results showed that nodule size had the most significant area under the curve (AUC = 0.665). Univariate and multivariate logistic regression analyses revealed that taller-than-wide shape ≥1, ill-defined margin, irregular shape, nodule size (≤1.40 cm), TT4 (>98.67 nmol/L), and FT3 (<4.14 pmol/L) were independent risk factors for BRAF^{V600E} mutation. While considering all these factors in the nomogram, the Concordance index (C-index) remained high at 0.764. This suggests that the model has a good predictive effect.

Abbreviations: PTC, Papillary Thyroid Cancer; TNM, Tumor Node Metastasis; TSH, thyroid-stimulating hormone; TT4, thyroxine; TT3, total-triiodothyronine; FT4, free thyroxine; FT3, free triiodothyronine; HE, hematoxylin and eosin; DNA, Deoxyribonucleic Acid; IQR, Interquartile Range; ROC, receiver operating characteristic; AUC, the area under the curve; CI, Confidence Interval; OR, odds ratio; C-Index, Consistency Index; AJCC, American Joint Committee on Cancer; PCR, Polymerase Chain Reaction; ARMS PCR, Amplification Refractory Mutation System-PCR; ddPCR, digital microdroplet PCR.

* Corresponding author. Department of Ultrasound, Guangxi Medical University Cancer Hospital, Guangxi Medical University, Nanning, 530021, Guangxi Zhuang Autonomous Region, China.
** Corresponding author. Department of Research, Guangxi Medical University Cancer Hospital, Guangxi Medical University, Nanning, 530021, Guangxi Zhuang Autonomous Region, China.
E-mail addresses: zhanglitu@gmail.com (L. Zhang), yangweiping@gxmu.edu.cn (W. Yang).
[1] These authors contributed equally to this work.

https://doi.org/10.1016/j.heliyon.2024.e29955
Received 1 February 2024; Received in revised form 17 April 2024; Accepted 17 April 2024
Available online 25 April 2024

Conclusion: Ultrasound features including nodule size, taller-than-wide shape ≥1, ill-defined margins, irregular shape, higher TT4 levels, and lower FT3 levels were associated with papillary thyroid cancer aggressiveness and BRAF^{V600E} mutation.

1. Introduction

Thyroid cancer is the most common malignant tumor of the endocrine system, accounting for 90 % of cases are papillary thyroid cancer [1,2]. It is more prevalent in women than in man [3]. The incidence of PTC has increased by about 6 % annually in recent years, making it a rapidly growing global malignancy [4]. The standard treatment for thyroid cancer is surgery combined with radioactive I^{131} ablation [5,6]. According to the source, while the treatment effect and prognosis for thyroid cancer patients are generally positive, there is a risk of recurrence and mortality due to regional and distant metastases, which occur in 6 %–20 % of case [7,8].

The BRAF^{V600E} mutation is the most common genetic mutation in thyroid cancer [9]. Studies suggest that patients with BRAF^{V600E} mutation may be associated with lymph node metastasis, vascular invasion, and distant metastasis, which increase the risk of disease recurrence [4,10]. Studies [11]have shown that BRAF^{V600E} mutations are more common in papillary than in follicular carcinoma. Therefore, the early detection of clinicopathological indicators related to BRAF^{V600E} mutation may provide a reference for selecting thyroid cancer treatment options, improving survival and prognosis.

The incidence of thyroid nodules in the general population is as high as 65 % [12], while the malignancy rate of thyroid nodules is 7%–15 % [13]. Ultrasound is an inexpensive and convenient modality, and ultrasonic features such as acoustic shadow, irregular margins, microcalcifications, and taller-than-wide shapes ≥1 have been used as potential predictors of malignant thyroid nodules [14–17]. Therefore, thyroid ultrasonography is essential for the initial evaluation of benign and malignant thyroid nodules [13].

Kabaker et al. [18,19] found that BRAF^{V600E} mutations were associated with malignant ultrasound features such as hypoechoic, irregular morphology, taller-than-wide shape ≥1, and microcalcifications of thyroid masses. However, the value of BRAF^{V600E} mutation in determining the aggressiveness of PTC and its correlation with ultrasound features is still controversial. This study takes advantage of retrospective analysis aimed investigating the value of BRAF^{V600E} mutation in determining the aggressiveness of PTC and its correlation with the ultrasound features of thyroid cancer nodules to improve the application of BRAF^{V600E} mutation detection in the management of PTC and to provide a better reference for the clinical diagnosis and treatment of PTC.

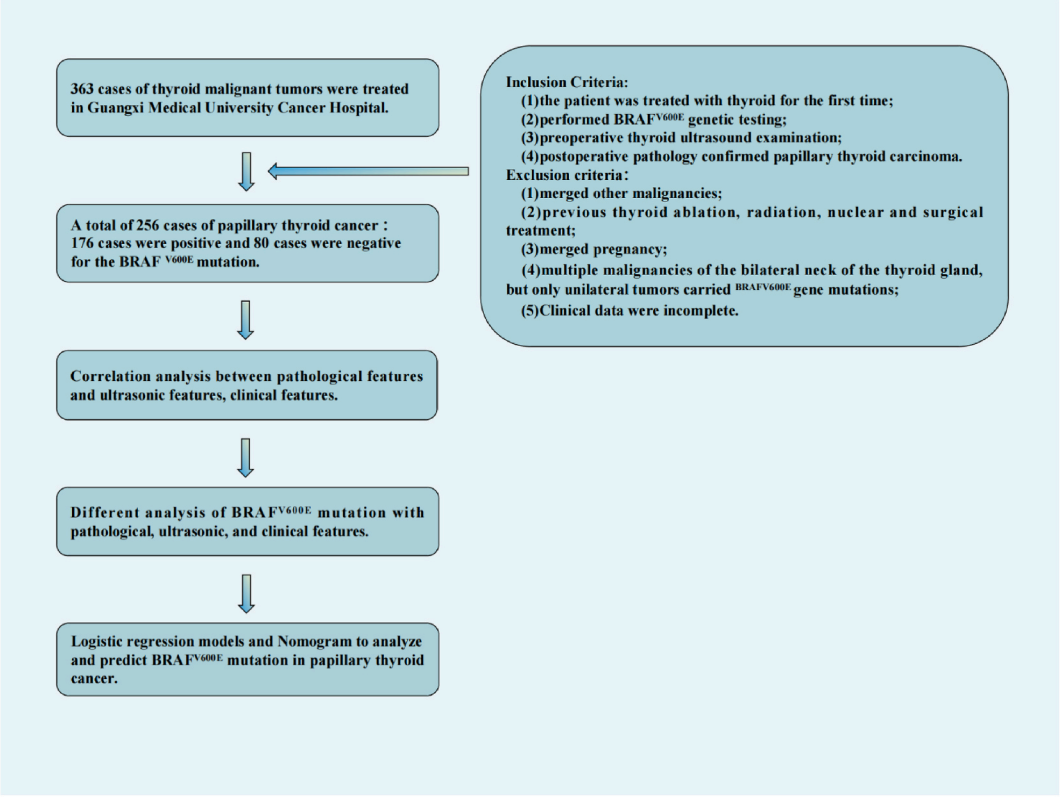

Fig. 1. Schematic diagram of this study.

Table 1
Baseline database of all the papillary thyroid cancer patients.

Features	Number	(%)
$BRAF^{V600E}$ mutation		
Positive (%)	176	(68.75 %)
Negative (%)	80	(31.25 %)
Gender		
Male (%)	71	(27.70 %)
Female (%)	185	(72.30 %)
Quantity		
Single (%)	185	(72.30 %)
Multiple (%)	71	(27.70 %)
Lymph node metastasis		
Positive (%)	103	(40.20 %)
Negative (%)	153	(59.80 %)
Nodular goiter		
Positive (%)	118	(46.10 %)
Negative (%)	138	(53.90 %)
Envelope invasion		
Positive (%)	119	(46.50 %)
Negative (%)	137	(53.60 %)
T stage		
T1 (%)	122	(47.66 %)
T2 (%)	13	(5.08 %)
T3 (%)	1	(0.39 %)
T4 (%)	120	(46.88 %)
N stage		
N0 (%)	153	(59.80 %)
N1 (%)	103	(40.20 %)
M stage		
M0 (%)	240	(93.25 %)
M1 (%)	16	(6.25 %)
Clinical stage		
I (%)	221	(86.33 %)
II(%)	13	(5.08 %)
III(%)	17	(6.64 %)
IV(%)	5	(1.95 %)
Location		
Left (%)	99	(38.70 %)
Right (%)	103	(40.20 %)
Isthmus (%)	8	(3.10 %)
Multiple (%)	46	(18.00 %)
Taller-than-wide shape		
<1 (%)	127	(49.60 %)
≥ 1 (%)	129	(50.40 %)
Composition		
Solid (%)	237	(92.60 %)
Mixed cystic and solid (%)	19	(7.40 %)
Margin		
Defined (%)	30	(11.70 %)
Ill-defined (%)	226	(88.30 %)
Shape		
Regular (%)	80	(31.30 %)
Irregular (%)	176	(68.80 %)
Echogenicity		
Hypoechoic (%)	235	(91.80 %)
Isoechoic (%)	2	(0.80 %)
Hyperechoic (%)	5	(2.00 %)
Mixed echoic (%)	14	(5.50 %)
Acoustic shadow		
Attenuation (%)	75	(29.30 %)
No acoustic shadow (%)	117	(45.70 %)
Enhancement (%)	64	(25.00 %)
Calcification		
Non-calcification (%)	77	(30.10 %)
Microcalcifications (%)	161	(62.90 %)
Macrocalcifications (%)	18	(7.00 %)
Adler Grade of blood flow		
Grade 0 (%)	15	(5.90 %)
Grade 1 (%)	102	(39.80 %)
Grade 2 (%)	93	(36.30 %)

(*continued on next page*)

Table 1 (*continued*)

Features	Number	(%)
Grade 3 (%)	46	(18.00 %)
Age (median [IQR])	41.50	[33–49.5]
Tumor size (median [IQR])	1.00	[0.6–1.5]
Nodule size (median [IQR])	1.10	[0.7–1.6]
TSH(median [IQR])	1.29	[0.81–1.78]
TT4 (median [IQR])	88.25	[78.14–101.48]
TT3 (median [IQR])	1.34	[1.18–1.48]
FT4 (median [IQR])	12.98	[12.17–14.08]
FT3 (median [IQR])	4.22	[3.84–4.56]

Abbreviation: Age, year; Tumor size, cm; Nodule size, cm; TSH, thyroid-stimulating hormone, μIU/ml; TT4, thyroxine, nmol/L; TT3, total-triiodothyronine, nmol/L; FT4, free thyroxine, pmol/L; FT3, free triiodothyronine, pmol/L; IQR, Interquartile Range.

2. Materials and methods

2.1. Research design

This study selected 256 PTC patients who underwent surgery at the Guangxi Medical University Cancer Hospital from May 2020 to June 2022. Inclusion criteria were as follows: (1) the patient underwent thyroid surgery for the first time; (2) $BRAF^{V600E}$ gene detection; (3) thyroid ultrasonic examination was performed in our hospital before surgery; and (4) Papillary thyroid cancer was pathologically diagnosed after surgery. The exclusion criteria were as follows: (1) combined with malignant tumors in other sites; (2) the patient has received radiofrequency ablation, nuclear therapy, neck radiotherapy, and other thyroid surgery; (3) pregnancy is present; (4) multiple malignant tumors in the left and right lobes of the thyroid gland have only a single mass $BRAF^{V600E}$ mutation, the general method is shown in Fig. 1. This study adhered to the ethical guidelines of the 2008 Declaration of Helsinki and was approved by the Ethics Committee of Guangxi Medical University Cancer Hospital (LW2023092).

2.2. Clinical data collection

In this retrospective study, we collected data on the clinicopathological characteristics of PTC patients. These data include gender, age, lymph node metastasis, envelope invasion, tumor size, TNM stage, clinical stage, $BRAF^{V600E}$ gene detection results, and contains thyroid-stimulating hormone (TSH), total-triiodothyronine (TT3), thyroxine (TT4), free triiodothyronine (FT3), free thyroxine (FT4) and other laboratory data. Hematological data were collected before treatment. In patients with multiple lesions, only the most significant lesion was analyzed. Finally, we included 256 patients who met the inclusion and exclusion criteria. Of these, 176 (68.75 %) were positive for $BRAF^{V600E}$ mutations, and 80 (31.25 %) were negative. The mean age of the patients was 41.50 ± 8.50 years. Among the 256 PTC patients, 221 (86.33 %) were in clinical stage I, 13 (5.08 %) were in clinical stage II, 17 (6.64 %) were in clinical stage III, and 5 (1.95 %) were in clinical stage IV. Table 1 shows the relevant pathological, ultrasonic, and clinical features.

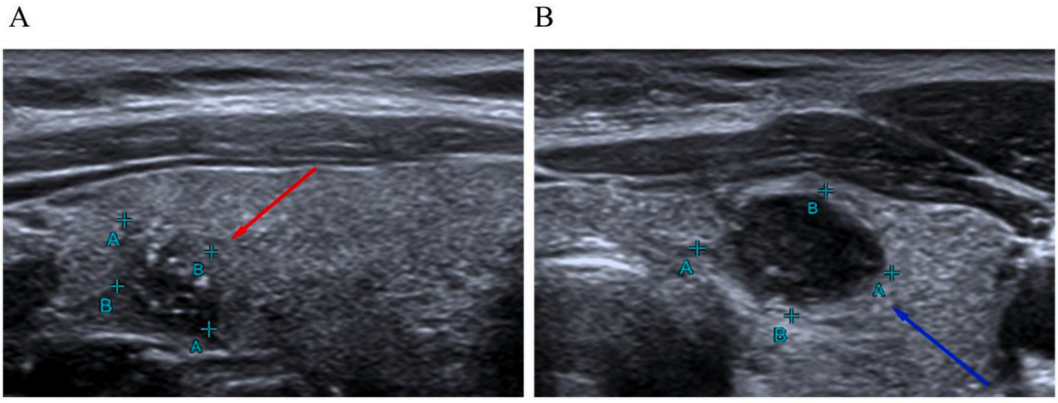

Fig. 2. The ultrasonic imaging features of PTC patients with $BRAF^{V600E}$ mutation A: $BRAF^{V600E}$ mutation positive: the nodule with ill-defined margin, the shape is irregular, taller-than-wide shape ≥1 (Red arrow in the Figure); B: $BRAF^{V600E}$ mutation negative: the nodule with defined margin, regular shape, taller-than-wide shape <1; (blue arrow). These ultrasonic nodules come from patients who were diagnosed as PTC pathologically. A+ and B+ are the long diameters and short diameters of the nodules. (For interpretation of the references to colour in this figure legend, the reader is referred to the Web version of this article.)

2.3. Conventional ultrasonic examination methods

Using Aplio400, Aplio500, and Aplio800 ultrasonic examiners manufactured by Toshiba Corporation (Japan) and LOGIQ E9 ultrasonic examiners manufactured by GE HealthCare (United States). A 14L5 high-frequency linear array probe with a 5–14 MHz frequency was selected. The patients were placed supine and fully exposed to the neck nodule. A routine ultrasonic examination of the thyroid gland was performed to record the following ultrasound features: nodule location, size, taller-than-wide shape, margin, shape, echogenicity, acoustic shadow, calcification, and extent of blood flow enhancement (judging by the Adler semi-quantitative method, Grace 0: No internal blood flow signal; Grade 1: a small amount of blood flow signal, 1–2 punctate blood flow can be seen; Grade 2: moderate blood flow signal, 3–4 punctate blood flow or 1 passing through blood vessels, the length of which may approach or exceed the radius of the lesion; Grade 3: blood flow signal is abundant, more than five punctate blood vessels or two long blood vessels can be seen). The physician interprets the results with more than ten years of experience in thyroid ultrasound diagnosis, and the ultrasound features are described without the physician knowing the pathological outcome of the thyroid lesions, which avoids subjective selection bias.

This study adheres to the guidelines [20] for diagnosing and treating thyroid cancer in the National Health Commission of the People's Republic of China. The guidelines identify microcalcification, irregular margins, and taller-than-wide shape ≥ 1 as the high specificity malignant signs of thyroid nodules. Other malignant symptoms include solid hypoechoic nodules, absent halos, extrathyroidal invasion, and cervical lymph node abnormalities. Fig. 2 (A-B) displays the results of following these guidelines in the study.

2.4. $BRAF^{V600E}$ genetic test

The pathologist selected the optimal wax block for genetic testing, ensuring the tumor tissue was more than 20 %. Deoxyribonucleic Acid (DNA) was extracted using Xiamen Adder Biomedical Technology Co., Ltd.'s nucleic acid extraction reagent (catalog number ADx-FF03). Gene mutation detection was performed using Xiamen Adder Biomedical Technology Co., Ltd.'s human $BRAF^{V600E}$ mutation detection kit (fluorescent polymerase chain reaction). The experimental operation was conducted strictly following the standard operating procedures of the Laboratory of Molecular Pathology, Department of Pathology, Cancer Hospital of Guangxi Medical University. Professional attending physicians of molecular pathology interpreted the results.

2.5. Pathological examination

This study analyzed 256 pathological specimens of goiter and cervical lymph nodes. The specimens were fixed using a 10 % neutral formaldehyde solution and processed using conventional dehydration, paraffin embedding, 4 μm sections, and hematoxylin and eosin (HE) staining. The pathologists who read the specimens have over ten years of experience in tumor diagnosis. The medical record includes information on the type and location of the cancer, its size and number, the presence of metastasis in cervical lymph nodes, the presence of concomitant nodular goiter, and whether the cancer has invaded the membrane.

2.6. Statistical analysis

Statistical analyses were performed using R statistical software (version 3.6.1), medical statistics software, and GraphPad Prism (version 9.4.1). Measurement parameters were tested for Kolmogorov-Smirnov normality, and the mean $\pm$ standard deviation ($x \pm s$) was used for normal distribution. The *t*-test was used to compare the two groups. Parameters not conforming to the normal distribution were tested using the Mann-Whitney *U* test, and the median $\pm$ interquartile range ($M \pm IQR$) was used for the non-normal distribution. Comparisons between census data groups were compared using the chi-squared test or Fisher's exact probability method. In this study, receiver operating characteristic (ROC) curves were constructed to determine the optimal cut-off and diagnostic accuracy for continuous variables. *P* value less than 0.05 (all two-tailed) are considered statistically significant. Characteristics with a *P* value less than 0.05 were included in the correlation model. All selected factors were used to develop a correlated nomogram model for $BRAF^{V600E}$ mutation risk in PTC patients. The nomograms were subjected to 1,000 boot strap resamples for internal validation. The consistency index (C-index) between correlation probability and response is used to evaluate the discrimination performance of the nomograms [21]. C-index values range from 0.5 to 1.0, with 0.5 representing random chance and 1.0 representing fully corrected discrimination [22]. Calibration is the ability of a model to produce an unbiased estimate of outcomes. We used the model's marginal estimate and average prediction probability to construct a calibration curve. The result will fall on the 45° diagonal line for a well-calibrated model.

3. Results

3.1. The nodule size is correlated with the tumor size of PTC

Tumor size in evaluating the extent of tumor invasion and predicting patient prognosis. Nodule size, TSH, TT4, TT3, FT4, and FT3 are critical indicators for assessing thyroid function. This study investigates the correlation between tumor size, nodule size, and thyroid function indicators grouped by $BRAF^{V600E}$ gene mutation status. The study found a linear correlation between tumor size and nodule size in both the mutant group ($R = 0.789$, $P < 0.001$) and the non-mutant group ($R = 0.623$, $P < 0.001$), as well as in the entire group ($R = 0.728$, $P < 0.001$). No linear correlation was observed between tumor size and TSH, TT4, TT3, FT4, or FT3. Furthermore, in

the absence of $BRAF^{V600E}$ mutation grouping, a linear correlation was observed between nodule size and TT4 (R = 0.196, $P = 0.002$), TT3 (R = 0.152, $P = 0.015$), FT4 (R = 0.178, $P = 0.004$), and FT3 (R = 0.168, $P = 0.007$), the results are shown in Fig. 3. The rest results are presented in Supplementary Table 62, and Supplementary Fig. 21.

3.2. The correlated analysis between $BRAF^{V600E}$ mutation and pathology, ultrasonic and other clinical categorical features in PTC

This study uses correlated analysis to investigate the correlation between $BRAF^{V600E}$ mutation and pathological, ultrasonic, and other clinical categorical features of PTC. The findings indicate that $BRAF^{V600E}$ mutation was negatively correlated with calcification and was positively correlated with taller-than-wide shape ≥1, ill-defined margin, and irregular shape (all $P < 0.05$). The results are shown in Table 2.

3.3. Differential analysis of ultrasound characteristics of $BRAF^{V600E}$ mutated and unmutated in PTC patients

The Mann-Whitney *U* test was used to analyze the difference between $BRAF^{V600E}$ mutations and PTC tumor size, nodule size, and thyroid hormone levels. The results showed a significant difference between $BRAF^{V600E}$ mutation and tumor size and nodule size (all $P < 0.05$), as shown in Fig. 4 (A-H). Additionally, the chi-square test was used to analyze the differences between $BRAF^{V600E}$ mutation and pathological, ultrasound, and other clinical features of PTC. The results indicate that the $BRAF^{V600E}$ mutation differed significantly from a taller-than-wide shape≥1, an ill-defined margin, and an irregular shape (all $P < 0.05$). These findings are presented in Fig. 5 (A-R).

3.4. Receiver operating characteristic curve (ROC curve)

This study examines the diagnostic effect of various clinical features, including tumor size, nodule size, TSH, TT4, TT3, FT4, FT3, on $BRAF^{V600E}$ mutation in PTC. Of all the ROC curves, the nodule size had the largest area under the curve (AUC = 0.665), as depicted in Fig. 6 (A-G). The study utilized the ROC curve (indexed by the Youden index) to determine the optimal cut-off value, diagnostic sensitivity, and specificity of clinical features that were correlated with $BRAF^{V600E}$ mutations. The results are presented in Table 3.

3.5. Construction of the univariate and multivariate logistic regression model

This study constructed the ROC curve to determine the optimal cut-off value of continuous characteristics for correlated with $BRAF^{V600E}$ mutations in PTC. Univariate logistic regression analysis was performed, and the results showed that tumor size, nodule

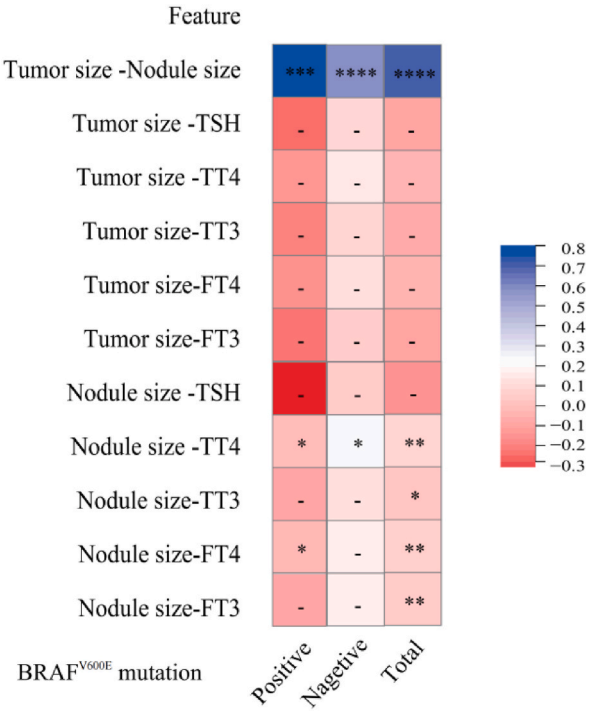

Fig. 3. The correlation analysis among tumor size, nodule size, and thyroid hormones The significance is marked as $P > 0.05$ NS; $P < 0.05$ *; $P < 0.01$ **; $P < 0.001$ ***; $P < 0.0001$ ****.

Table 2
Correlation analysis of $BRAF^{V600E}$ mutation and clinical features in PTC.

Features	R	*P* value
Gender	−0.004	0.955
Quantity	−0.091	0.148
Lymph node metastasis	−0.031	0.620
Nodular goiter	0.066	0.296
T stage	−0.066	0.294
N stage	−0.031	0.620
M stage	**0.000**	1.000
Clinical stage	0.058	0.358
Location	−0.002	0.973
Taller-than-wide shape	0.342	**< 0.001**
Composition	−0.002	0.974
Margin	0.226	**< 0.001**
Shape	0.255	**< 0.001**
Echogenicity	−0.104	0.097
Acoustic shadow	0.041	0.511
Calcification	−0.145	**0.020**
Adler Grade of blood flow	−0.011	0.860

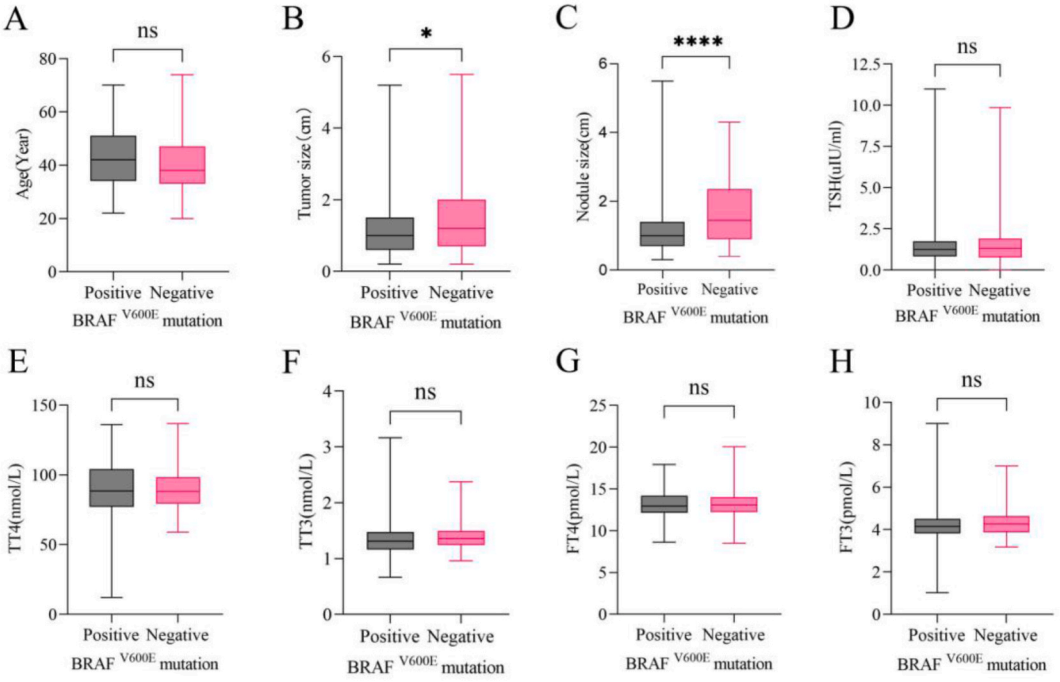

Fig. 4. The difference analysis among tumor size, nodule size, and thyroid hormones. A: Age differences in $BRAF^{V600E}$ mutations; B: Tumor size differences in $BRAF^{V600E}$ mutations; C: Nodule size differences in $BRAF^{V600E}$ mutations; D: TSH differences in $BRAF^{V600E}$ mutations; E: TT4 differences in $BRAF^{V600E}$ mutations; F: TT3 differences in $BRAF^{V600E}$ mutations; G: FT4 differences in $BRAF^{V600E}$ mutations; H: FT3 differences in $BRAF^{V600E}$ mutations; The significance is marked as $P > 0.05$ NS; $P < 0.05$ *; $P < 0.01$ **; $P < 0.001$ ***; $P < 0.0001$ ****.

size, TT4, TT3, and FT3 were correlated with $BRAF^{V600E}$ mutation (all $P < 0.05$). This indicates that tumor size, nodule size, TT4, TT3, and FT3 may be risk factors for $BRAF^{V600E}$ mutation in PTC. Additionally, ultrasonic characteristics such as taller-than-wide shape, margin, and morphology related to $BRAF^{V600E}$ mutation were obtained using either the Chi-square test or the Fisher exact test. However, a linear relationship was observed between nodule size and tumor size, TT4 and TT3. Furthermore, the area under the curve of nodule size was the largest (AUC = 0.665). Therefore, when constructing the logistic regression model in this study, we included risk factors other than tumor size and TT3. The results indicated that nodule size, taller-than-wide shape, margin, TT4, and FT3 were independent risk factors for $BRAF^{V600E}$ mutation (all $P < 0.05$). The results are shown in Table 4.

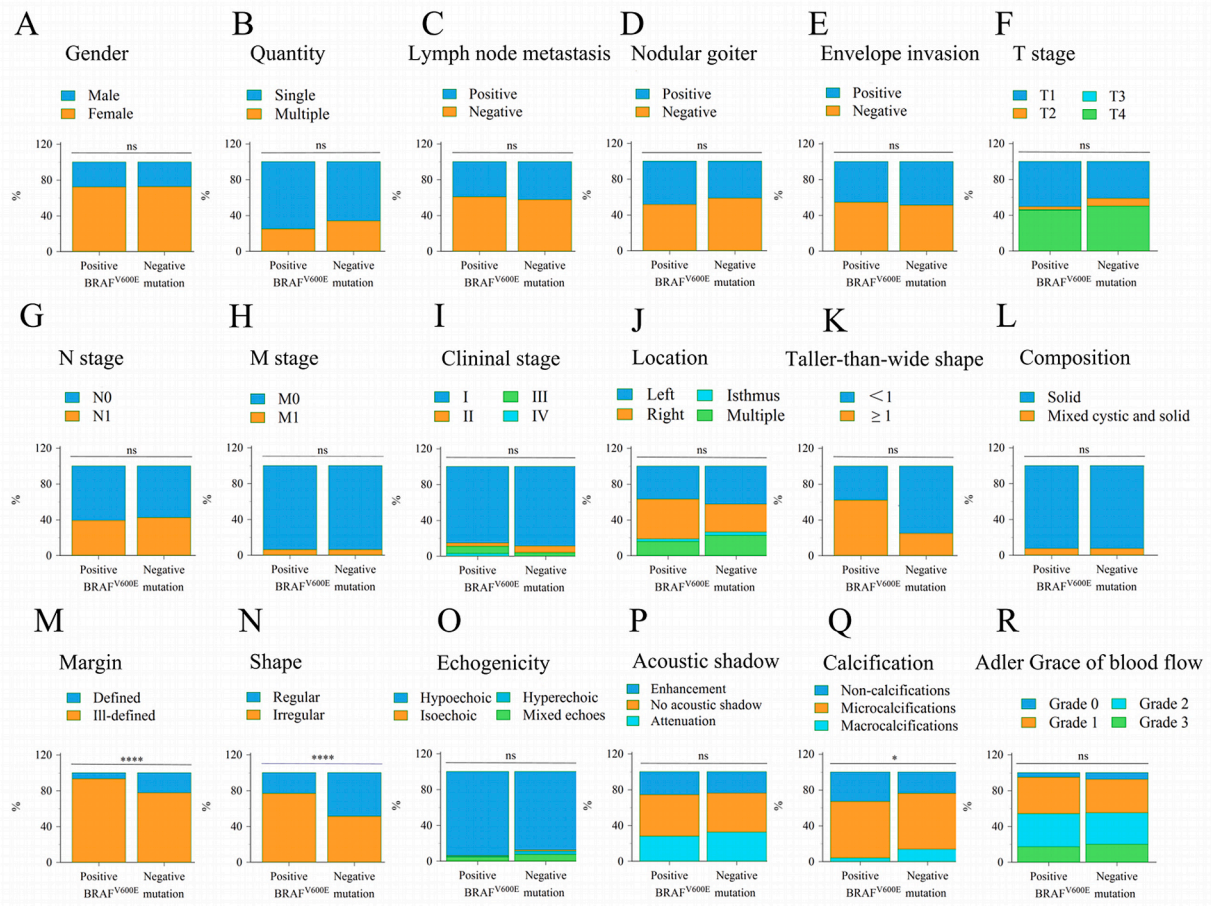

Fig. 5. The difference analysis among $BRAF^{V600E}$ mutation and pathology and ultrasonic and other clinical feature A–I: The difference analysis among $BRAF^{V600E}$ mutation and pathology and clinical feature; J–R: The difference analysis between $BRAF^{V600E}$ mutation and ultrasonic feature; The significance is marked as $P > 0.05$ NS; $P < 0.05$ *; $P < 0.01$ **; $P < 0.001$ ***; $P < 0.0001$ ****.

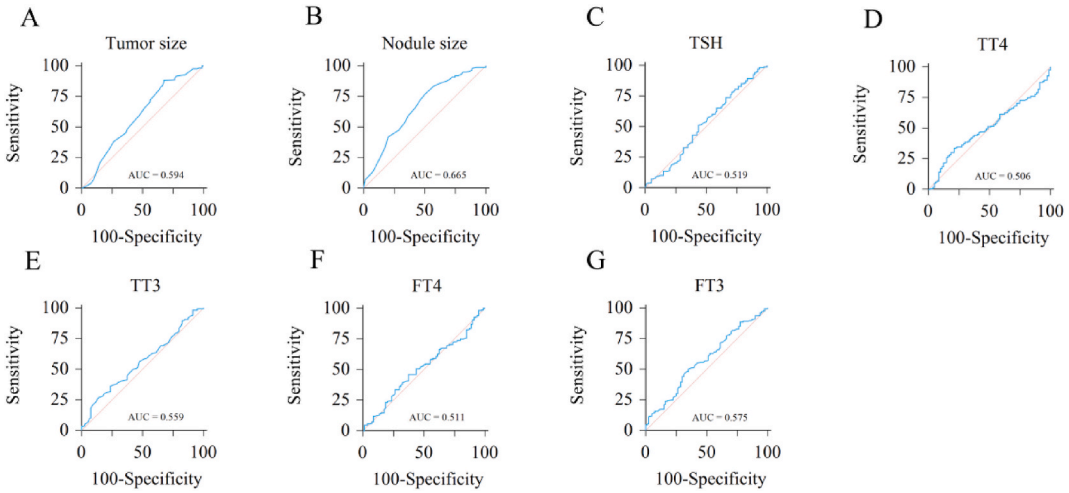

Fig. 6. Area under the curve (AUC) of $BRAF^{V600E}$ mutation in PTC. A: Tumor size; B: Nodule size; C: TSH; D: TT4; E: TT3; F: FT4; G: FT3.

Table 3
ROC curve analysis.

Features	AUC(95%CI)	Threshold	*P* value	Sensitivity	Specificity	Youden
Tumor size	0.594 (0.531–0.654)	1.90	**0.019**	88.070	32.500	0.206
Nodule size	0.665 (0.603–0.722)	1.40	**< 0.001**	76.700	50.000	0.267
TSH	0.519 (0.455–0.581)	1.60	0.647	73.860	33.750	0.076
TT4	0.506 (0.443–0.569)	98.67	0.864	33.520	78.750	0.123
TT3	0.559 (0.496–0.621)	1.17	0.119	26.700	86.250	0.130
FT4	0.511 (0.448–0.573)	14.20	0.785	75.570	15.000	0.094
FT3	0.575 (0.511–0.536)	4.14	0.053	50.000	65.000	0.150

Abbreviation: Tumor size, cm; Nodule size, cm; TSH, thyroid-stimulating hormone,μIU/ml; TT4, thyroxine, nmol/L; TT3, total-triiodothyronine, nmol/L; FT4, free thyroxine, pmol/L; FT3, free triiodothyronine, pmol/L; ROC, receiver operating characteristic; AUC, the area under the curve.

Table 4
Univariate and Multivariate logistics regression analysis.

Variable	Univariate logistics regression analysis			Multivariate logistics regression analysis		
	OR	95 % CI	*P* Value	OR	95 % CI	*P* Value
Tumor size	3.554	1.8494–6.8289	**< 0.001**			
Nodule size	3.293	1.8797–5.7677	**< 0.001**	2.166	1.1048–4.2460	**0.014**
TSH	1.440	0.8121–2.5523	0.212			
TT4	1.869	1.0049–3.4753	**0.048**	2.492	1.2010–5.1722	**0.048**
TT3	2.333	1.1074–4.9164	**0.026**			
FT4	0.546	0.2701–1.1030	0.092			
FT3	1.735	1.0045–2.9957	**0.048**	1.908	1.0065–3.6166	**< 0.001**
Taller-than-wide shape	4.881	2.7041–8.8089	**< 0.001**	3.680	1.8891–7.1671	**0.032**
Margin	3.968	1.8066–8.7140	**0.001**	2.790	1.0911–7.1358	**0.003**
Shape	3.132	1.7879–5.4869	**< 0.001**	2.658	1.3863–5.0971	**< 0.001**
Macrocalcifications	0.221	0.0788–0.6222	**0.004**			

Abbreviation: Tumor size, cm; Nodule size, cm; TSH, thyroid-stimulating hormone,μIU/ml; TT4, thyroxine, nmol/L; TT3, total-triiodothyronine, nmol/L; FT4, free thyroxine, pmol/L; FT3, free triiodothyronine, pmol/L; CI, Confidence Interval; OR, odds ratio.

3.6. Construction of a nomogram model that correlates factors with the BRAF^{V600E} mutation

We constructed a nomogram based on independent risk factors from multivariate logistic regression analysis. The results showed that the taller-than-wide shape contributed the most to correlating with BRAF^{V600E} mutations in PTC, followed by margin, shape, TT4, and finally, nodule size and FT3. The C-index was 0.764, and the predicted value is 0.837, as shown in Fig. 7 (A). The calibration curve shows that the BRAF^{V600E} mutation correlation curve is consistent, and the model is well calibrated, and the results are shown in Fig. 7 (B).

3.7. Subgroup logistics regression analysis of various factors on BRAF^{V600E} mutation in different environments

We performed subgroup logistic regression analysis to exclude confounding factors according to TNM stage, clinical stage, and independent risk factors. We explored each factor's predictive effect on BRAF^{V600E} mutation in different settings. The results show that compared with the T1-T2 stage, tumor size (OR = 5.525) and margin (OR = 3.123) were independent risk factors for BRAF^{V600E}

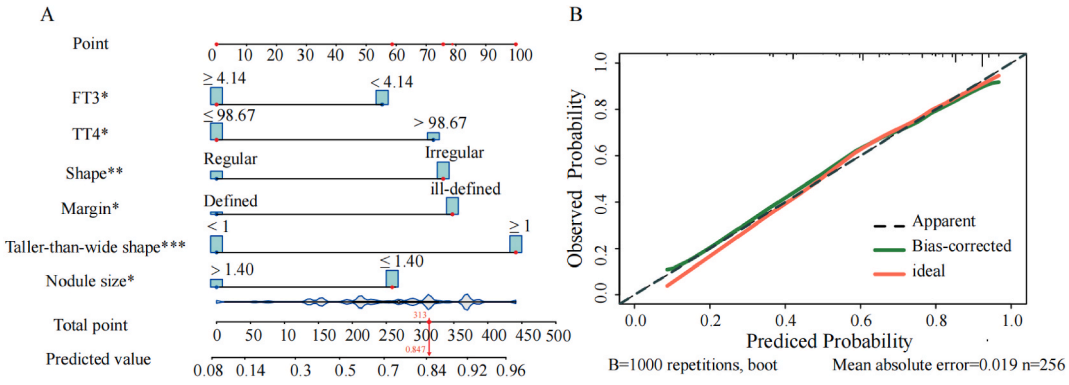

Fig. 7. Nomogram model and calibration curve B–A: Nomogram model; Nodule size, cm; TT4, thyroxine, nmol/L; FT3, free triiodothyronine, pmol/L; $P > 0.05$ NS; $P < 0.05$ *; $P < 0.01$ **; $P < 0.001$ ***; $P < 0.0001$ ****. B: calibration curve.

Table 5
Multivariate logistics regression analysis of different TNM stages, clinical stages and independent risk factors in PTC.

Multivariate logistics regression analysis				
Group	Variable	OR	95 % CI	*P* value
T1-T2 stage				
	Taller-than-wide shape	5.525	2.3486–12.9964	**< 0.001**
	Shape	3.123	1.3507–7.2227	**0.008**
T3-T4 stage				
	Tumor size	2.515	1.2118–5.2191	**0.013**
	Taller-than-wide shape	4.463	2.3819–8.3623	**< 0.001**
	Margin	2.713	1.0812–6.8047	**0.034**
	Shape	2.448	1.2957–4.6266	**0.006**
N0 stage				
	Nodule size	2.895	1.2437–6.7399	**0.014**
	Taller-than-wide shape	3.669	1.5809–8.5145	**0.003**
	Shape	3.287	1.4768–7.3143	**0.004**
N1 stage				
	FT3	3.265	1.0380–10.2702	**0.043**
	Taller-than-wide shape	3.589	1.3623–9.4553	**0.010**
	Margin	7.942	1.5664–40.2668	**0.012**
M0 stage				
	Tumor size	2.687	1.2047–5.9938	**0.016**
	TT4	2.768	1.2780–5.9954	**0.010**
	FT3	2.118	1.0930–4.1055	**0.026**
	Taller-than-wide shape	3.888	2.0288–7.4502	**< 0.001**
	Margin	2.688	1.0446–6.9171	**0.040**
	Shape	2.417	1.2389–4.7167	**0.010**
I-II stage				
	Tumor size	2.633	1.1824–5.8613	**0.018**
	Taller-than-wide shape	4.706	2.4315–9.1095	**< 0.001**
	Margin	2.984	1.1324–7.8653	**0.027**
	Shape	2.265	1.1712–4.3810	**0.015**
Taller-than-wide shape <1				
	Nodule size	2.217	1.0143–4.8441	**0.046**
	Margin	4.122	1.3332–12.7472	**0.014**
	Shape	3.184	1.4240–7.1186	**0.005**
Taller-than-wide shape ≥1				
	TT4	5.738	1.7991–18.3015	**0.003**
	Shape	4.335	1.2990–14.4670	**0.017**
	Quantity	0.279	0.0891–0.8731	**0.028**
	Microcalcifications	5.836	1.1752–28.9767	**0.031**
Defined Margin				
	Nodule size	3.301	1.7162–6.3483	**< 0.001**
	Shape	0.285	0.1584–0.5127	**< 0.001**
ill-defined Margin				
	Tumor size	3.028	1.4523–6.3127	**0.003**
	TT4	2.294	1.0491–5.0167	**0.038**
	Taller-than-wide shape	4.172	2.2398–7.7698	**<0.001**
	Shape	3.040	1.6335–5.6587	**0.001**
Regular Shape				
	TSH	5.235	1.4478–18.9305	**0.012**
	TT4	9.228	1.3976–60.9258	**0.021**
	Taller-than-wide shape	4.398	1.1544–16.7560	**0.030**
	Margin	8.435	1.7458–40.7495	**0.008**
Irregular Shape				
	Taller-than-wide shape	4.347	1.9706–9.5870	**<0.001**
	Macrocalcifications	0.146	0.0319–0.6689	**0.013**
Nodule size >1.4 cm				
	Taller-than-wide shape	6.294	1.3667–28.9830	**0.018**
	Shape	5.177	1.5717–17.0486	**0.007**
	Microcalcifications	10.362	2.1429–50.1047	**0.007**
Nodule size ≤1.4 cm				
	TT4	3.238	1.0380–10.0985	**0.043**
	Taller-than-wide shape	2.885	1.3627–6.1094	**0.006**
	Shape	2.554	1.1752–5.5509	**0.018**
TT4 > 98.67 nmol/L				
	FT3	14.060	1.9725–100.2241	**0.008**
	Taller-than-wide shape	10.664	2.1375–53.2053	**0.004**
TT4 ≤ 98.67 nmol/L				
	Nodule size	2.944	1.2676–6.8389	**0.012**
	FT4	3.292	1.5519–6.9837	**0.002**
	Taller-than-wide shape	3.387	1.5331–7.4839	**0.003**

(*continued on next page*)

Table 5 (*continued*)

	Margin	4.076	1.9249–8.6326	**< 0.001**
FT3 ≥ 4.14 pmol/L				
	TT3	6.870	1.2606–37.4374	**0.026**
	Taller-than-wide shape	5.111	2.2102–11.8188	**< 0.001**
	Shape	3.592	1.5760–8.1876	**0.002**
FT3 < 4.14 pmol/L				
	Nodule size	6.759	2.2436–20.3600	**0.001**
	TT4	6.486	1.3140–32.0100	**0.022**
	Gender	0.196	0.0399–0.9618	**0.045**

Abbreviation: Tumor size, cm; Nodule size, cm; TSH, thyroid-stimulating hormone,μIU/ml; TT4, thyroxine, nmol/L; TT3, total-triiodothyronine, nmol/L; FT4, free thyroxine, pmol/L; FT3, free triiodothyronine, pmol/L; OR, odds ratio; TNM, Tumor Node Metastasis.

mutation in the T3-T4 stage. Compared with the M0 and I–II stages, there were no independent risk factors for $BRAF^{V600E}$ mutation in the M1 and III–IV stages, respectively. The remaining results are shown in Table 5. The rest results are shown in Supplementary Table 1 to Table 61, and Supplementary Fig. 1 to Fig. 20 (A-G).

4. Discussion

The BRAF gene belongs to a class of oncogenes. Most mutations occur in the 1799th nucleotide of exon 15, resulting in the replacement of valine with glutamic acid in the 600th codon of protein translation, which causes abnormal phosphorylation, activates the MAPK signaling pathway, regulates cell proliferation and differentiation, and promotes tumorigenesis and development [23,24]. Some studies have suggested that $BRAF^{V600E}$ mutations are associated with aggressive behavior and adverse prognosis, such as multiple carcinomas, lymphatic metastasis, membrane invasion, high TNM stage, and prognosis [25–28]. However, some studies suggest that $BRAF^{V600E}$ mutations are not significantly associated with prognosis [29,30]. In this study, we included 176 patients with $BRAF^{V600E}$ mutation and 80 patients without mutation and performed a correlation analysis between pathology features and $BRAF^{V600E}$ mutation in PTC patients. The results showed that tumor size was significantly correlated with the $BRAF^{V600E}$ gene mutation ($P = 0.016$), consistent with the results of Kwak et al. [25,31,32]. However, multiple cancer lesions, lymphoid metastasis, membrane invasion, TNM stage, and clinical stage were not significantly correlated with $BRAF^{V600E}$ mutations, which may be related to sample size and population distribution.

Furthermore, most previous studies used the American Joint Committee on Cancer (AJCC) seventh edition staging criteria, and this study used the AJCC 8th edition staging criteria to stage PTC. Lechner [33] noted differences in survival prognosis between patients following AJCC 7th and 8th edition staging criteria. At the same time, Tam [34] concluded that the survival prognosis of patients using these two staging criteria was similar. This suggests that for the survival prognosis of patients with thyroid cancer, the use of different versions of the AJCC staging criteria may lead to different outcomes. While Pontius' study observed this difference, Tam's findings implied a similarity between the two staging criteria regarding survival prognosis. However, further studies are needed to understand and explain this phenomenon due to such differences and similarities.

Thyroid ultrasonography is the first step in thyroid cancer screening and diagnosis, and the wide application of thyroid ultrasound and fine needle aspiration has significantly improved the detection rate of thyroid cancer. Whether non-invasive ultrasonography can be used to evaluate the molecular expression of thyroid cancer at an early stage is of great significance for preoperative evaluation of the lesions' aggressiveness, prognosis, and the selection of reasonable treatment options. However, the value of $BRAF^{V600E}$ mutation in determining the aggressiveness of PTC and its correlation with ultrasound features is still controversial. Previous studies [25,35] have believed that $BRAF^{V600E}$ gene mutations are not significantly correlated with ultrasound features. Conversely, Kabaker [18,19] et al. believed that ultrasound features such as unclear boundaries, hypoechoic, microcalcification, non-cystic composition, and absence of a halo are significantly associated with $BRAF^{V600E}$ gene mutations. In 2006, Boelaert [36] first reported a correlation between TSH levels and the occurrence of thyroid cancer. However, the correlation analysis between thyroid hormones $BRAF^{V600E}$ gene mutations is rare. In this study, we conducted correlation analysis and univariate and multivariate logistics regression analysis. The results of multivariate analysis showed that the ultrasound features of nodule size, taller-than-wide shape, ill-defined margin, irregular shape, and higher level TT4 and lower level FT3 were independent risk factors for $BRAF^{V600E}$ gene mutation. This is similar to the findings of Kabaker [18,19,37,38] et al. The correlation analysis between ultrasound nodule size and $BRAF^{V600E}$ gene mutation was rare. Park [35] believed that the increase in cancer lesion size was associated with $BRAF^{V600E}$ gene mutation, while ultrasound nodule size was not correlated with $BRAF^{V600E}$ gene mutation. In this study, we performed linear correlation analysis. We found a significant correlation between cancer lesion size and ultrasound nodule size ($P < 0.05$); the cut-off values of tumor size and ultrasound nodule size correlated with $BRAF^{V600E}$ gene mutation were <1.90 cm and 1.40 cm, respectively. Subsequent univariate logistics regression analysis showed significant correlations between cancer lesion size and ultrasound nodule size, as well as $BRAF^{V600E}$ gene mutation, consistent with the study of Kwak [31,32] et al. The presence of multiple nodules and multiple malignant tumors increases the heterogeneity of the sample and may lead to complications during data analysis. The inconsistency of these results may be related to the interference error caused by the multiple occurrences of nodules and carcinoma. Chen [37,38] et al. believed multiple tumors significantly correlated with $BRAF^{V600E}$ gene mutations. Still, our results showed that single or multiple tumors had no significant correlation with $BRAF^{V600E}$ mutations ($P = 0.148$), consistent with Ahn's study [29]. In addition, The main research population of this study was single nodules (72.30 %), which not only ensured the matching degree of nodules and cancer but also avoided the

interference error caused by multiple cancers.

Finally, we used the six independent risk factors obtained by multivariate regression analysis to construct the nomogram and perform calibration curve analysis on the nomogram, which showed that the six independent risk factors have a reasonable correlation with the $BRAF^{V600E}$ gene mutation. However, the $BRAF^{V600E}$ gene mutation correlation model that has been reported is rare. In this study, we explored the correlation of pathological, ultrasound, and clinical features on $BRAF^{V600E}$ gene mutations in PTC and developed a nomogram that contains ultrasound features and clinical features.

Ultrasound detection is a convenient, economical, and harmless examination method. The development of high-resolution ultrasound has made significant progress in PTC's detection rate and diagnostic specificity. Ultrasound-guided fine-needle aspiration cytology is currently the standard method for diagnosing thyroid cancer before surgery, and its specificity is high, but there is still a misdiagnosis rate of 15 %~25 %. In addition, as a highly accurate molecular diagnostic technology, genetic testing plays a crucial role in diagnosing hereditary diseases, predicting disease risk and guiding personalized treatment. Standard genetic testing methods include Amplification Refractory Mutation System-PCR (ARMS PCR) and digital microdroplet PCR (ddPCR), characterized by high precision and accuracy. In addition, next-generation sequencing (NGS) is characterized by high throughput, comprehensiveness, and versatility. It can sequence DNA fragments simultaneously, making it suitable for various genomes, transcriptomes, and epigenome sequencing types. However, the high cost of genetic testing technology, the need for specialized equipment, and the complexity of operating techniques limit its widespread use in primary care and disease screening.

Therefore, there is an urgent need for a means that can be widely used in risk screening for tumors. Combining with previous studies, we have integrated ultrasound features and serum thyroid hormones into an easy-to-use nomogram that can tell the relationship between Ultrasound and $BRAF^{V600E}$ mutations of PTC. The internal validation in the cohort shows good discrimination and calibration ability, especially the interval validation C-index (0.764), which indicates that the correlation model can be widely used. This is the first time a nomogram has been combined with thyroid ultrasound features and thyroid hormones for risk assessment and correlation of $BRAF^{V600E}$ gene mutations. This borderline assessment approach allows clinicians and high-risk patients to quickly and easily obtain personalized risk profiles. This finding is unique because it combines ultrasonographic features, clinical indicators, and molecular biomarkers to provide a relatively accurate tool for diagnosing thyroid cancer.

However, this study also had some limitations. First, the study was retrospective; all specimens were from a single institution for postoperative thyroid cancer cases, with some selection bias. However, we developed a severe standard to reduce the selection bias. Second, the accuracy of our nomogram should be evaluated through external validation, which will help to assess whether our nomogram applies to new populations. Follow-up studies will be externally validated, and large-scale clinical trials are needed to illustrate and improve the model's effectiveness in predicting $BRAF^{V600E}$ mutations in PTC. Third, the postoperative follow-up time of the subjects was short, and all patients were still alive, so survival analysis could not be performed. Subsequent studies will continue to explore the relationship between $BRAF^{V600E}$ mutation and the survival prognosis in PTC. Finally, we will refine the diagnostic models and cost-effectiveness analyses and improve their clinical utility.

5. Conclusion

In conclusion, our systematic and comprehensive analysis determined that Ultrasound features, including nodule size, taller-than-wide shape $\geq$1, ill-defined margins, irregular shape, higher TT4 levels, and lower FT3 levels were associated with papillary thyroid cancer aggressiveness and $BRAF^{V600E}$ mutation. The simple operation and preferential price make this correlation method can be more widely used in primary hospitals. Quantifying preoperative thyroid ultrasound and thyroid function tests may help physicians better evaluate the risk of $BRAF^{V600E}$ gene mutation in PTC patients. This is of great significance for treatment selection and prognosis evaluation.

Ethical declaration

All methods were carried out in accordance with the Declaration of Helsinki. This project fully considered and protected the rights and interests of the study objects. It meets the criteria of Ethical Review Committee. The Medical Ethics Committee of Guangxi Medical University Cancer Hospital has approved the protocol. Approval Number: LW2023092.

Data availability statement

This published article and its supplementary information files include all data generated or analyzed during this study. The corresponding author can provide all possible assistance to the requester of the original data.

Funding

This study was supported by grants from the Key R&D Program of Scientific Research and Technology Development Project of Guangxi (Grant No. Gui Ke AB23026078), the Key R&D Program of Scientific Research and Technical Development Project of Qingxiu District, Nanning, Guangxi (Grant No. 2021015) and Guangxi Medical and health key discipline construction project.

CRediT authorship contribution statement

Jiahao Wen: Writing – original draft. **Haizhou Liu:** Writing – review & editing, Data curation, Conceptualization. **Yanyan Lin:** Writing – original draft. **Zixuan Liang:** Data curation. **Lili Wei:** Data curation. **Qi Zeng:** Data curation. **Shanshan Wei:** Data curation. **Litu Zhang:** Writing – review & editing, Methodology, Conceptualization. **Weiping Yang:** Methodology.

Declaration of competing interest

The authors declare that they have no known competing financial interests or personal relationships that could have appeared to influence the work reported in this paper.

Acknowledgement

This work was supported by the Guangxi Cancer Hospital Biological Resource Bank for providing the samples.

Appendix A. Supplementary data

Supplementary data to this article can be found online at https://doi.org/10.1016/j.heliyon.2024.e29955.

References

[1] A. Acuña-Ruiz, C. Carrasco-López, P. Santisteban, Genomic and epigenomic profile of thyroid cancer, Best Pract. Res. Clin. Endocrinol. Metabol. 37 (1) (2023) 101656, https://doi.org/10.1016/j.beem.2022.101656.
[2] C. Pizzimenti, V. Fiorentino, A. Ieni, M. Martini, G. Tuccari, M. Lentini, et al., Aggressive variants of follicular cell-derived thyroid carcinoma: an overview, Endocrine 78 (1) (2022) 1–12, https://doi.org/10.1007/s12020-022-03146-0.
[3] L.F. Remer, C.I. Lee, O. Picado, J.I. Lew, Sex differences in papillary thyroid cancer, J. Surg. Res. 271 (2022) 163–170, https://doi.org/10.1016/j.jss.2021.11.004.
[4] X. Wei, X. Wang, J. Xiong, C. Li, Y. Liao, Y. Zhu, et al., Risk and prognostic factors for BRAFV600E mutations in papillary thyroid carcinoma, BioMed Res. Int. 2022 (2022) 9959649, https://doi.org/10.1155/2022/9959649. Published 2022 May 18.
[5] M.E. Cabanillas, D.G. McFadden, C. Durante, Thyroid cancer, Lancet. 388 (10061) (2016) 2783–2795, https://doi.org/10.1016/S0140-6736(16)30172-6.
[6] F. Nabhan, P.H. Dedhia, M.D. Ringel, Thyroid cancer, recent advances in diagnosis and therapy, Int. J. Cancer 149 (5) (2021) 984–992, https://doi.org/10.1002/ijc.33690.
[7] L. Shobab, K.D. Burman, L. Wartofsky, Sex differences in differentiated thyroid cancer, Thyroid 32 (3) (2022) 224–235, https://doi.org/10.1089/thy.2021.0361.
[8] E.F.S. van Velsen, R.P. Peeters, M.T. Stegenga, U. Mäder, C. Reiners, F.J. van Kemenade, et al., Tumor size and presence of metastases in differentiated thyroid cancer: comparing c=ohorts from two countries, Eur. J. Endocrinol. 188 (6) (2023) 519–525, https://doi.org/10.1093/ejendo/lvad061.
[9] X. Goh, J. Lum, S.P. Yang, S.B. Chionh, E. Koay, L. Chiu, et al., BRAF mutation in papillary thyroid cancer-Prevalence and clinical correlation in a South-East Asian cohort, Clin. Otolaryngol. 44 (2) (2019) 114–123, https://doi.org/10.1111/coa.13238.
[10] R.P. Tufano, G.V. Teixeira, J. Bishop, K.A. Carson, M. Xing, BRAF mutation in papillary thyroid cancer and its value in tailoring initial treatment: a systematic review and meta-analysis, Medicine (Baltim.) 91 (5) (2012) 274–286, https://doi.org/10.1097/MD.0b013e31826a9c71.
[11] A. Chakraborty, A. Narkar, R. Mukhopadhyaya, S. Kane, A. D'Cruz, M.G. Rajan, BRAF V600E mutation in papillary thyroid carcinoma: significant association with node metastases and extra thyroidal invasion, Endocr. Pathol. 23 (2) (2012) 83–93, https://doi.org/10.1007/s12022-011-9184-5.
[12] C. Durante, G. Grani, L. Lamartina, S. Filetti, S.J. Mandel, D.S. Cooper, The diagnosis and management of thyroid nodules: a review [published correction appears in JAMA. 2018 Apr 17;319(15):1622], JAMA 319 (9) (2018) 914–924, https://doi.org/10.1001/jama.2018.0898.
[13] R. Wong, S.G. Farrell, M. Grossmann, Thyroid nodules: diagnosis and management, Med. J. Aust. 209 (2) (2018) 92–98, https://doi.org/10.5694/mja17.01204.
[14] L. Zhang, T. Yin, B. Li, R. Zheng, C. Qiu, K.S. Lam, et al., Size-modulable nanoprobe for high-performance ultrasound imaging and drug delivery against cancer, ACS Nano 12 (4) (2018) 3449–3460, https://doi.org/10.1021/acsnano.8b00076.
[15] T. Rago, P. Vitti, Risk stratification of thyroid nodules: from ultrasound features to TIRADS, Cancers 14 (3) (2022) 717, https://doi.org/10.3390/cancers14030717. Published 2022 Jan 30.
[16] P. Prieditis, M. Radzina, M. Mikijanska, M. Liepa, K. Stepanovs, G. Grani, et al., Non-marked hypoechogenic nodules: multicenter study on the thyroid malignancy risk stratification and accuracy based on TIRADS systems comparison, Medicina (Kaunas) 58 (2) (2022) 257, https://doi.org/10.3390/medicina58020257. Published 2022 Feb 9.
[17] Q. Chen, M. Lin, S. Wu, Validating and comparing C-TIRADS, K-TIRADS and ACR-TIRADS in stratifying the malignancy risk of thyroid nodules, Front. Endocrinol. 13 (2022) 899575, https://doi.org/10.3389/fendo.2022.899575. Published 2022 Jun 17.
[18] A.S. Kabaker, M.E. Tublin, Y.E. Nikiforov, M.J. Armstrong, S.P. Hodak, M.T. Stang, et al., Suspicious ultrasound characteristics predict BRAF V600E-positive papillary thyroid carcinoma, Thyroid 22 (6) (2012) 585–589, https://doi.org/10.1089/thy.2011.0274.
[19] E.J. Lee, K.H. Song, D.L. Kim, Y.M. Jang, T.S. Hwang, S.K. Kim, The BRAF(V600E) mutation is associated with malignant ultrasonographic features in thyroid nodules, Clin. Endocrinol. 75 (6) (2011) 844–850, https://doi.org/10.1111/j.1365-2265.2011.04154.
[20] J. Zhou, L. Yin, X. Wei, et al., 2020 Chinese guidelines for ultrasound malignancy risk stratification of thyroid nodules: the C-TIRADS, Endocrine 70 (2) (2020) 256–279, https://doi.org/10.1007/s12020-020-02441-y.
[21] S. Yang, H. Zhou, C. Feng, N. Xu, Y. Fan, Z. Zhou, et al., Web-based nomograms for overall survival and cancer-specific survival of bladder cancer patients with bone metastasis: a retrospective cohort study from SEER database, J. Clin. Med. 12 (2) (2023) 726, https://doi.org/10.3390/jcm12020726. Published 2023 Jan 16.
[22] M.J. Pencina, RB Sr D'Agostino, R.B. D'Agostino Jr., R.S. Vasan, Evaluating the added predictive ability of a new marker: from area under the ROC curve to reclassification and beyond, Stat. Med. 27 (2) (2008) 157–212, https://doi.org/10.1002/sim.2929.
[23] M. Xing, BRAF mutation in papillary thyroid cancer: pathogenic role, molecular bases, and clinical implications, Endocr. Rev. 28 (7) (2007) 742–762, https://doi.org/10.1210/er.2007-0007.
[24] L. Maji, G. Teli, N.M. Raghavendra, S. Sengupta, R. Pal, A. Ghara, et al., An updated literature on BRAF inhibitors (2018-2023), Mol. Divers. (2023), https://doi.org/10.1007/s11030-023-10699-3. Published online July 20.

[25] X. Zheng, S. Wei, Y. Han, Y. Li, Y. Yu, X. Yun, et al., Papillary microcarcinoma of the thyroid: clinical characteristics and BRAF(V600E) mutational status of 977 cases, Ann. Surg Oncol. 20 (7) (2013) 2266–2273, https://doi.org/10.1245/s10434-012-2851-z.
[26] L. Zhu, X. Zhang, S. Zhang, Q. Zhang, L. Cao, Y. Zhang, et al., Cancer-associated fibroblasts in papillary thyroid carcinoma, Clin. Exp. Med. 23 (6) (2023) 2209–2220, https://doi.org/10.1007/s10238-023-00998-2.
[27] L. Zhao, R. Jiang, M. Xu, P. Zhu, X.M. Mo, N. Wang, et al., Concomitant high expression of BRAFV600E, P-cadherin and cadherin 6 is associated with High TNM stage and lymph node metastasis in conventional papillary thyroid carcinoma, Clin. Endocrinol. 84 (5) (2016) 748–755, https://doi.org/10.1111/cen.12878.
[28] G. Elia, A. Patrizio, F. Ragusa, S.R. Paparo, V. Mazzi, E. Balestri, et al., Molecular features of aggressive thyroid cancer, Front. Oncol. 12 (2022) 1099280, https://doi.org/10.3389/fonc.2022.1099280. Published 2022 Dec 20.
[29] D. Ahn, J.S. Park, J.H. Sohn, J.H. Kim, S.K. Park, A.N. Seo, et al., BRAFV600E mutation does not serve as a prognostic factor in Korean patients with papillary thyroid carcinoma, Auris Nasus Larynx 39 (2) (2012) 198–203, https://doi.org/10.1016/j.anl.2011.07.011.
[30] S.Y. Choi, H. Park, M.K. Kang, D.K. Lee, K.D. Lee, H.S. Lee, et al., The relationship between the BRAF(V600E) mutation in papillary thyroid microcarcinoma and clinicopathologic factors, World J. Surg. Oncol. 11 (2013) 291, https://doi.org/10.1186/1477-7819-11-291. Published 2013 Nov 14.
[31] J.Y. Kwak, E.K. Kim, W.Y. Chung, H.J. Moon, M.J. Kim, J.R. Choi, Association of BRAFV600E mutation with poor clinical prognostic factors and US features in Korean patients with papillary thyroid microcarcinoma, Radiology 253 (3) (2009) 854–860, https://doi.org/10.1148/radiol.2533090471.
[32] J.A. Silver, M. Bogatchenko, M. Pusztaszeri, V.I. Forest, M.P. Hier, J.W. Yang, et al., BRAF V600E mutation is associated with aggressive features in papillary thyroid carcinomas $\leq$ 1.5 cm, J Otolaryngol Head Neck Surg 50 (1) (2021) 63, https://doi.org/10.1186/s40463-021-00543-9. Published 2021 Nov 6.
[33] M.G. Lechner, A.C. Bernardo, A. Lampe, S.S. Praw, S.H. Tam, T.E. Angell, Changes in stage distribution and disease-specific survival in differentiated thyroid cancer with transition to American Joint Committee on cancer 8th edition: a systematic review and meta-analysis, Oncol. 26 (2) (2021) e251–e260, https://doi.org/10.1634/theoncologist.2020-0306.
[34] S. Tam, M. Boonsripitayanon, M. Amit, B.M. Fellman, Y. Li, N.L. Busaidy, et al., Survival in differentiated thyroid cancer: comparing the AJCC cancer staging seventh and eighth editions, Thyroid 28 (10) (2018) 1301–1310, https://doi.org/10.1089/thy.2017.0572.
[35] A.Y. Park, E.J. Son, J.A. Kim, J.H. Youk, Y.J. Park, C.S. Park, et al., Associations of the BRAF(V600E) mutation with sonographic features and clinicopathologic characteristics in a large population with conventional papillary thyroid carcinoma, PLoS One 9 (10) (2014) e110868, https://doi.org/10.1371/journal.pone.0110868. Published 2014 Oct 22.
[36] K. Boelaert, J. Horacek, R.L. Holder, J.C. Watkinson, M.C. Sheppard, J.A. Franklyn, Serum thyrotropin concentration as a novel predictor of malignancy in thyroid nodules investigated by fine-needle aspiration, J. Clin. Endocrinol. Metab. 91 (11) (2006) 4295–4301, https://doi.org/10.1210/jc.2006-0527.
[37] B. Chen, Z. Zhang, K. Wang, M. Shang, S. Zhao, W. Ding, Association of BRAFV600E mutation with ultrasonographic features and clinicopathologic characteristics of papillary thyroid microcarcinoma: a retrospective study of 116 cases, Clin. Hemorheol. Microcirc. 73 (4) (2019) 545–552, https://doi.org/10.3233/CH-190568.
[38] K.L. Lin, O.C. Wang, X.H. Zhang, X.X. Dai, X.Q. Hu, J.M. Qu, The BRAF mutation is predictive of aggressive clinicopathological characteristics in papillary thyroid microcarcinoma, Ann. Surg Oncol. 17 (12) (2010) 3294–3300, https://doi.org/10.1245/s10434-010-1129-6.